Astronomy Reports, Vol. 44, No. 6, 2000, pp. 353–364. Translated from Astronomicheskiĭ Zhurnal, Vol. 77, No. 6, 2000, pp. 407–419.
Original Russian Text Copyright © 2000 by Gorshkov, Konnikova, Mingaliev.

Analysis of Instantaneous Spectra of a Complete Sample of Flat-Spectrum Radio Sources

A. G. Gorshkov[1], V. K. Konnikova[1], and M. G. Mingaliev[2]

[1]*Sternberg Astronomical Institute, Universitetskiĭ pr. 13, Moscow, 119899 Russia*

[2]*Special Astrophysical Observatory, Russian Academy of Sciences, Nizhniĭ Arkhyz, Karachaevo-Cherkesskaya Republic, 357147 Russia*

Received May 5, 1999

Abstract—The results of observations of a complete sample of radio sources with spectral indices $\alpha > -0.5$ ($S \propto \nu^{\alpha}$) are presented. The sample was selected from the Zelenchuk Survey at 3.9 GHz and contains all sources with declinations 4°–6°, Galactic latitudes $|b| > 10°$, and 3.9-GHz fluxes > 200 mJy. Spectra at 0.97–21.7 GHz were obtained for all 69 sample sources. The spectra were classified, and a correlation between variability amplitude and spectrum shape was found. The spectra were separated into extended and compact components. The distribution of spectral indices α for the extended components coincides with the distribution for sources with power-law spectra. The correlation between the luminosity and frequency of the peak flux density is confirmed. This correlation is due to the fact that the distribution of source linear dimensions does not depend on luminosity. *© 2000 MAIK "Nauka/Interperiodica".*

1. INTRODUCTION

Many radio sources with spectral indices $\alpha > -0.5$ ($S \propto \nu^{\alpha}$) have complex morphologies. We also classify objects whose spectra cannot be described by a power law over a wide frequency range and whose two-frequency spectral index at centimeter wavelengths is > –0.5 as flat-spectrum sources. In such sources, along with the emission of extended structures, an appreciable, and often dominant, fraction of the emission comes from very compact structures with angular sizes less than one arcsec. In some objects, these compact components are not resolved by VLBI on the largest baselines available on the Earth's surface. These compact structures are identified with active galactic nuclei (AGN) and the "central machines" that are ultimately responsible for the radio emission.

Nonstationary processes that take place in AGN result in variations of the flux densities of radio sources on various timescales, from days to decades. After the detection of variability in discrete sources in 1966 [1, 2], this phenomenon has been actively studied at many observatories. Long-term series of observations of large samples of radio sources at decimeter [3], centimeter [4, 5], and millimeter [6] wavelengths have been obtained. Detailed studies of the most remarkable representatives of this class of objects are also carried out (see, for example, [7]).

During the last 1.5 years, we have been studying the variability of sources with flat spectra over a wide frequency range. For this purpose, we observed sources in a complete sample selected from the 3.9-GHz Zelenchuk Survey [8]. The sample includes all sources with 3.9-GHz flux densities $S_{3.9} \geq 200$ mJy with declinations 4°–6° and Galactic latitudes $|b| > 10°$. The sample contains 161 sources, of which 69 objects (43%) have flat spectra ($\alpha_{(3.9\text{–}7.7\ \mathrm{GHz})} > -0.5$). We presented an analysis of the spectra of the sample sources with spectral indices $\alpha_{(3.9\text{–}7.7\ \mathrm{GHz})} \leq -0.5$ (steep spectra) in [9]. Based on RATAN-600 monitoring in 1985–1992 at 3.9 and 7.5 GHz, we found that only 14 of the 69 flat-spectrum sample sources did not display significant variability during the observation period [10].

The purpose of the present work is to study the spectral parameters of compact components and their possible connection with the character of the variability. The spectra of the variable sources change with time; therefore, studies of instantaneous spectra require measurements that are simultaneous or separated by intervals much shorter than the variability timescales, as well as measurements of the spectra over a wide frequency range. We consider the source spectra averaged over a time interval of 15 to 50 days and derive variability parameters from five observational sessions carried out over a year and a half.

2. OBSERVATIONS

The observations of the sample sources were carried out on the meridian on the RATAN-600 radio telescope simultaneously at six frequencies: 0.97, 2.3, 3.9, 7.7, 11.1, and 21.7 GHz. The parameters of the receivers used on the Northern sector of RATAN-600 are given in [11, 12]. The antenna beam parameters are presented in [9]. Nearly all the spectra were obtained in August and November 1997 and January–February 1998. The

1063-7729/00/4406-0353$20.00 © 2000 MAIK "Nauka/Interperiodica"

spectra of seven sources were measured in May 1997 and of two, in August 1996. In each series, the sources were observed daily for 15–30 days, except for the January–February 1998 series, when the sources were observed over 50 days.

In addition to the flat-spectrum sources, we observed sources with steep spectra and constant flux densities (no less than 40% of all the sources observed). We used these objects as reference sources in our variability study, to eliminate instrumental effects, and to calibrate the flux densities of the target sources. The flux densities of all sources were statistically calibrated against the flux densities for the constant sources listed in [9]. The flux density of a source was determined as the weighted-mean value obtained using all the data in each observational series. The error of the weighted-mean flux density is defined to be

$$\Delta S = [\Sigma(S_i - \langle S\rangle)^2/(N-1)]^{0.5},$$

where S_i is the flux density for a given day, $\langle S\rangle$ is the weighted-mean flux density, and N is the number of observations of the source in the series. This error includes all sources of error: noise, calibration errors, calibration-signal reference errors, antenna pointing errors, etc.

3. INVESTIGATION OF THE SPECTRA

Table 1 lists the measured flux densities of the flat-spectrum sources studied at declinations 4°–6°. Column 1 gives the source name; columns 2, 4, 6, 8, 10, and 12, the source flux densities at 0.97, 2.3, 3.9, 7.7, 11.1, and 21.7 GHz; columns 3, 5, 7, 9, 11, and 13, the errors in the flux densities at these frequencies; and column 14, the epoch of the observation.

Classification of the spectra. The spectra of all 69 sources were fit with a parabola on a logarithmic scale using a least-squares method. Examination of the spectra and their least-squares fits showed that the spectra at 3–23 GHz can be divided into five types, as shown in Fig. 1:

(1) Spectra with flux densities that grow with frequency (growing spectra; Fig. 1a).

(2) Spectra with a flux-density minimum (Fig. 1b).

(3) Spectra with flux densities that decrease with frequency (Fig. 1c).

(4) Spectra that cannot be satisfactorily fit with a parabola (complex spectra; Fig. 1d).

(5) Spectra with a flux-density maximum (Fig. 1e).

All these types of spectra except for type 4 are well approximated by a parabola; in the overwhelming majority of cases, the differences between the measured and approximated flux densities are within two sigma. Spectra of types 1 and 3 have a small positive or negative curvature. In three cases, the best fit is a straight line.

The complex and type-5 spectra have a flux-density maximum in the frequency range considered, but in complex spectra, this maximum is usually located at higher frequencies. In these spectra, a local minimum is often observed in addition to a maximum.

Table 2 lists the parameters of the sources belonging to different types. Column 1 gives the spectrum type; column 2, the number of sources of the given type and the fraction (in percent) they constitute of the entire sample; column 3, the number of sources in which variability was detected over 1.5 years and the mean variability index; and column 4, the mean redshifts of the sources.

Relation between type of spectrum and variability. All of the sample sources were observed at six frequencies over 1.5 years (in three to five sessions). Statistically significant flux density variations were detected in 26 of the 69 sources. For each of these sources, we calculated the variability index $\bar{V} = \Delta S/\langle S\rangle$, representing the mean relative amplitude of the variability for our observation period. The definition of $\bar{V}$ and the procedure for our calculations are given in [13].

It follows from the data of Table 2 that the number of variable sources and their mean relative variability amplitude depend on the spectrum type. All six sources with type 1 (growing) spectra showed significant variability during the 1.5-year observation period, with mean amplitude $\bar{V} = 0.32$. Among the type-2 sources (with a minimum in their spectra), 40% were variable, with mean variability amplitude $\bar{V} = 0.31$. Variability with mean amplitude $\bar{V} = 0.24$ was found in one-third of the sources with type-3 spectra. Variable sources with $\bar{V} = 0.26$ made up 40% of type-4 sources (with complex spectra). Only two of the 16 sources with type-5 spectra had flux densities that were variable over the 1.5-year observation period, with mean variability amplitude $\bar{V} = 0.12$.

We believe that sources with spectra of types 1 and 2 are at an early stage of development of an outburst; the flux-density maximum is at millimeter wavelengths in the source frame, and type-2 sources have a considerable extended component. Sources of types 3 and 4 are at a later stage of development of a flare. The difference between these types of spectra could be related to the different contributions of their extended components (greater in type 3) or to sources with type-3 spectra being at a later phase of their activity compared to sources of type 4. It is likely that a considerable fraction of sources with spectra of types 1–4 represent a single class of object that are at different stages of development of their activity.

Sources with spectra of type 5 differ from the remaining sources in the nearly complete absence of variable objects among them and the very narrow range of frequencies ν_{max} where the maximum flux density is attained (see below, Fig. 4, the shaded area of the histogram); the extended component in these sources is faint

Table 1. Flux densities of the radio sources, mJy

Name	Frequency, GHz												Epoch*
	0.97		2.3		3.9		7.7		11.1		21.7		
	S	σ	S	σ	S	σ	S	σ	S	σ	S	σ	
1	2	3	4	5	6	7	8	9	10	11	12	13	14
0002 + 051	123	10	164	9	237	6	203	7	180	7	130	12	4
0019 + 058	262	15	268	9	279	8	306	5	310	6	274	27	3
0026 + 048	501	12	429	6	417	5	370	5	341	8	262	11	4
0027 + 056	275	19	367	10	422	9	498	7	524	6	541	31	3
0119 + 041	941	16	1138	7	1368	10	1613	15	1696	17	1499	28	5
0146 + 056	592	22	1034	20	1256	11	1417	10	1360	14	986	35	3
0152 + 043	360	19	368	13	356	9	285	6	261	7	150	15	3
0231 + 045	302	12	327	9	304	5	252	6	215	5	133	15	2
0237 + 040	954	14	825	6	748	7	625	6	600	10	492	23	5
0258 + 058	348	30	355	8	342	7	309	6	266	6	186	13	3
0303 + 051			202	9	283	6	228	7	191	8	60	29	2
0320 + 045	245	21	149	5	132	3	105	4	97	5	107	10	5
0348 + 049	751	19	510	8	387	12	297	5	250	5	187	15	4
0351 + 045	430	14	331	6	344	5	278	4	252	7	146	17	5
0355 + 055	80	16	182	11	256	9	276	7	234	6	139	20	3
0357 + 057	306	24	360	11	387	9	470	18	497	13	417	32	2
0409 + 044	127	8	203	5	229	4	226	4	200	5	140	12	5
0423 + 051	337	20	589	7	561	6	472	6	420	8	346	18	5
0425 + 048	902	18	576	12	534	15	504	8	498	14	577	23	4
0430 + 052	4160	30	3950	25	3870	19	4455	37	4380	54	2990	143	3
0502 + 049	1015	13	971	8	845	7	780	6	724	11	599	25	5
0506 + 056	376	23	435	13	485	9	595	10	604	16	463	33	3
0718 + 042	243	11	219	4	310	5	434	5	532	9	610	31	5
0731 + 050	271	10	268	5	270	4	291	3	322	6	345	14	5
0801 + 044	330	12	264	11	269	11	188	7	185	8	87	26	3
0805 + 046	579	13	465	5	478	4	449	7	426	9	304	13	5
0806 + 059	612	17	341	10	275	5	209	7	194	9	177	26	2
0829 + 046	1018	15	966	11	980	8	1248	11	1462	16	1703	47	5
0830 + 040	352	22	246	18	269	9	340	7	392	8	370	22	3
0858 + 050	119	14	192	5	250	4	309	4	343	7	388	15	5
1013 + 054	373	11	215	4	163	3	147	4	170	6	238	19	5
1015 + 057	427	23	530	13	608	9	778	19	893	20	883	40	2
1036 + 054	413	12	470	5	554	7	693	7	743	12	713	32	5
1117 + 044	314	15	276	9	252	4	232	10	228	6	161	12	3
1142 + 052	805	14	496	6	421	6	350	5	361	8	367	19	5
1204 + 057	559	18	396	13	351	10	340	14	339	9	294	20	2
1219 + 054	379	22	235	10	190	12	178	6	184	9	102	18	3
1219 + 044	684	25	529	9	578	8	822	10	1073	10	1946	53	4
1228 + 045	285	18	313	9	302	6	295	6	287	8	316	20	4
1237 + 049	396	18	444	6	430	5	443	5	462	9	483	23	5
1358 + 046	351	16	233	13	202	7	168	5	153	6	105	27	3

Table 1. (Contd.)

1	2	3	4	5	6	7	8	9	10	11	12	13	14
1402 + 044	866	18	1064	7	1024	9	1058	9	1081	16	959	21	5
1421 + 048	209	22	197	9	176	5	172	6	181	8	190	14	4
1456 + 044	1226	16	842	7	837	8	924	8	1006	20	1378	44	5
1509 + 054	40	13	177	4	407	5	783	7	906	13	799	31	5
1541 + 050	296	39	269	9	274	6	278	6	278	10	234	19	3
1542 + 042	937	25	577	16	438	7	352	7	392	12	442	28	4
1548 + 056	2200	50	2463	23	3193	24	3980	28	3948	54	2898	92	3
1557 + 043	289	13	189	5	159	3	163	4	172	6	182	14	5
1614 + 051	266	22	615	7	851	7	866	8	734	12	476	24	5
1614 + 042	375	18	226	15	203	5	141	6	119	8	76	20	2
1642 + 054	750	22	439	7	295	6	235	5	214	7	175	15	5
1646 + 042	595	66	290	13	250	4	199	6	175	8	169	16	4
1656 + 053	1844	22	1378	12	1225	9	1245	9	1172	14	927	34	5
1725 + 044	598	20	620	8	778	9	1180	18	1303	36	1342	46	4
1758 + 046	88	26	244	17	255	9	229	9	201	7	193	26	1
1926 + 050	453	14	334	6	314	7	298	6	284	5	224	16	4
1936 + 046	586	26	453	6	412	4	427	5	406	12	418	21	5
2019 + 050	168	14	416	6	464	5	400	5	342	7	218	18	5
2114 + 048	316	24	263	6	259	4	335	5	381	9	441	20	4
2121 + 053	540	35	545	14	700	20	1178	24	1641	38	2219	113	3
2144 + 042	85	44	98	11	123	5	160	14	214	5	236	23	1
2149 + 056	484	17	868	20	902	9	792	8	700	7	465	28	2
2201 + 044	896	25	554	12	470	16	385	6	378	10	372	22	4
2243 + 047	633	16	388	5	405	8	399	8	399	8	387	15	4
2259 + 058	177	14	295	8	322	10	336	7	324	6	235	18	3
2318 + 049	659	13	695	7	846	7	956	8	1073	28	1308	47	4
2346 + 052	697	17	451	14	366	11	416	7	400	10	297	28	3
2355 + 042	254	24	207	5	188	3	190	4	210	7	236	18	5

* (1) August 1996, (2) May 1997, (3) August 1997, (4) November 1997, (5) January–February 1998.

(or absent). The mean peak frequency in the observer's frame is 6.87 GHz. Nine objects of this group are identified with quasars; their mean redshift, $\bar{z} = 2.03$, is nearly twice that of the sources of other spectral types. For the quasars, the mean peak frequency in the observer's frame virtually coincides with $\bar{\nu}_{max}$ for all of group 5. Therefore, we believe that most sources with type 5 spectra are distant, luminous quasars with a small range of redshifts. The variability timescale in the source frame is 3–4 years; for a mean redshift $\bar{z} \approx 2$, this is 9–12 years in the observer's frame, and changes in flux density will be insignificant over 1.5 years. Furthermore, it was shown in [10] that the variability amplitude decreases with increasing luminosity.

There are probably also distant quasars among the sources with complex spectra, however, with extended components. Note that variability is absent in sources with type-4 spectra in objects with $\nu_{max} < 7$ GHz.

To study the spectra of the compact components, we must isolate their spectra; i.e., remove the emission of the extended component.

Separation of the components. We assume that all the spectra consist of two components: a power-law component,

$$\log S = S_0 + \alpha \log \nu \quad (1)$$

and a compact component, which can be represented by a quadratic function

$$\log S = C + (\log \nu - B)^2/2A, \quad (2)$$

where C is the logarithm of the flux density at the maximum of the spectrum, B is the logarithm of the frequency of this maximum, and A is the logarithmic inter-

val from the peak frequency to the frequency where $d(\log S)/d(\log \nu) = 1$ (the spectral curvature). It was shown in [14] that the spectra of compact components are well represented by formula (2) over a wide range of frequencies. We separated the components as follows. We chose the best-fit solution

$$\Sigma[S_{\nu i} - (S^s_{\nu i} + S^c_{\nu i})]^2,$$

where $S_{\nu i}$ is the flux density measured at a given frequency, $S^s_{\nu i}$ is the flux density for the power-law component, and $S^c_{\nu i}$ is the flux density for the compact component. For sources with data at frequencies below 0.97 GHz, we also found fits using these data.

Figure 2 shows an example of the separation into components for the source 0805 + 046; the diamonds show the initial spectrum, the solid curve shows the compact component, and the dashed curve shows the extended component.

We managed to separate into components all 39 sources with spectra of types 4 and 5 and two of the nine sources with spectra of type 3; the flux densities of the compact components peak at frequencies not exceeding 23 GHz. We found no extended components in three sources. For the remaining 28 sources, we could not separate the components. There could be several reasons for this: First, more than one compact component could be present; second, the compact component could be very faint or absent; third, the frequency of the spectral maximum for the compact component could be much higher than the maximum frequency of our measurements.

Figure 3 shows the spectral-index distribution for the extended components we have distinguished. The mean spectral index $\bar{\alpha}$ is –0.87, and the distribution standard deviation $\sigma_{\bar{\alpha}}$ is 0.15. The mean index and character of the distribution are similar to parameters obtained for samples of constant sources with power-law spectra [9, 10]. This supports the correctness of our component separation.

At our lowest observation frequency, 0.97 GHz, the variable component of the flux density of the compact component strongly depends on the shape of the total spectrum: For type-5 spectra with maxima in the frequency range considered, this variable component constitutes from 35 to 100% of the total (i.e., absence of an extended component). For this type of spectra, the mean contribution of the compact component to the integrated flux density at 0.97 GHz is 75%.

For type-4 (complex) spectra, the fraction of the 0.97-GHz total flux density contributed by the compact component seldom exceeds 35% (the mean fraction is 25%). At 0.365 GHz, for most sources, the variable component contributes less than 10%.

Spectra of the compact components. Table 3 lists characteristics of 41 sources in which the spectra of the compact components peak at 3–23 GHz. We approximated the spectra using formula (2). Table 3 presents the source (1) name; (2), (3) right ascension and declination at epoch 1950.0; (4) identification; (5) redshift; (6) flux density (mJy) at the maximum of the spectrum; (7) frequency (GHz) for this maximum; and (8) spectral curvature (*A*). We derived these quantities using only our data at frequencies from 0.97 to 21.7 GHz.

Table 2. Source parameters as a function of spectrum type

Spectrum type	Number of sources of given type (percent of total)	Number of sources displaying variability in 1.5 years (mean variability amplitude $\bar{V}$)	Mean redshift of quasars *z* (number of objects)
1	2	3	4
1	6 (9%)	6 (0.32)	
2	15 (22%)	6 (0.31)	1.3 (7)
3	9 (13%)	3 (0.24)	
4	22 (31%)	9 (0.26)	1.2 (9)
5	17 (25%)	2 (0.12)	2.03 (9)

For sources with flux densities measured at lower frequencies (in the Texas Survey at 365 MHz, the Molonglo Survey at 408 MHz, or the Arecibo Survey at 611 MHz), we also approximated the spectra using these data. For most of the sources, the results of this approximation were close to those in Table 3. For example, the differences in the peak frequencies did not exceed 5%. This rather good agreement of the approximation coefficients also testifies to the correctness of our separation of the emission into components.

Figure 4 presents the distribution of the peak frequencies for the 41 sources listed in Table 3. The sources that had type-5 spectra prior to the component separation are shaded. The mean peak frequency for the distribution $\bar{\nu}_{max}$ is 9 GHz, with a standard deviation σ of 5 GHz.

Of the 41 sources, 18 objects are quasars with known redshifts, three are galaxies, and three are BL Lac objects. The mean peak frequency for the quasars $\bar{\nu}_{max}$ (QSO) is 8.65 GHz, with σ = 5.7 GHz. For sources identified with star-like objects and empty fields (i.e., objects with magnitudes fainter than 21), $\bar{\nu}_{max}$ is 8.8 GHz. The coincidence of the $\bar{\nu}_{max}$ values for the quasars and objects with unknown *z* suggests that the latter are primarily quasars with a mean redshift close to that of the known quasars in our sample. Therefore, we take the spectral characteristics of the known quasars to be typical of the sample of radio sources. For the sources identified with BL Lac objects and galaxies, $\bar{\nu}_{max}$ (L + G) is 10.8 GHz, with σ = 1.8 GHz; therefore, we infer that,

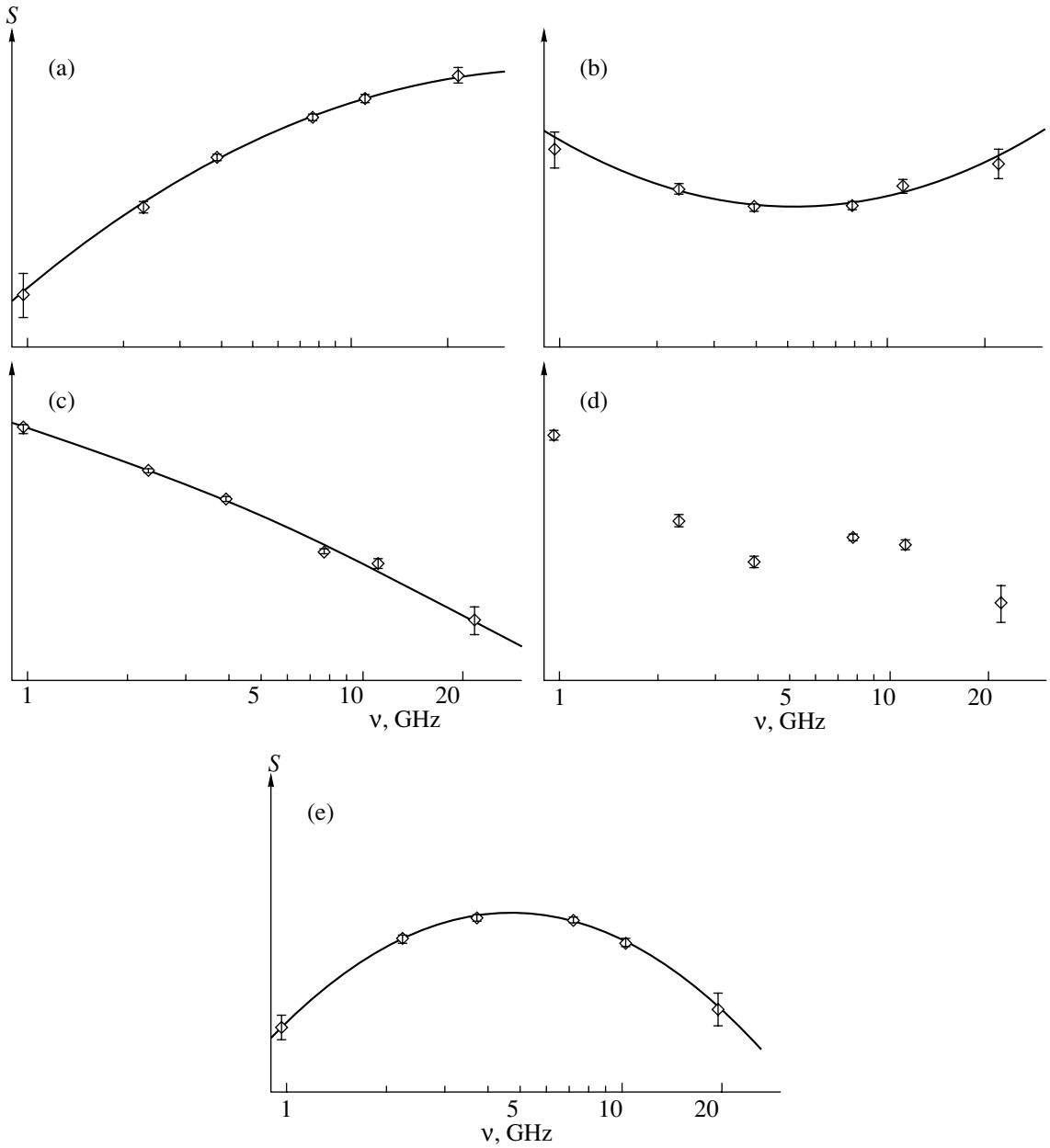

Fig. 1. Forms of spectra for the complete sample of radio sources with spectral indices $\alpha > -0.5$ (flat spectra). The vertical scale is in arbitrary units.

among the objects with unknown z, the (L + G) fraction is close to that among the identified sources.

Parameters of the spectra of compact components. Figure 5 shows the spectral characteristics of the compact components (diamonds: quasars, crosses: BL Lac objects and galaxies) as a function of redshift. For the BL Lac objects, we adopted $z = 0.5$. Figure 5a presents the absolute spectral radio luminosity at the peak frequency in a homogeneous, isotropic cosmological model with zero cosmological constant, deceleration parameter $q_0 = 0.5$, and $H = 50$ km s^{-1} Mpc^{-1}. The dashed line designates the minimum luminosity that can be detected for sources in our flux-density-limited sample; the straight-line segment shows the cutoff of the quasar luminosity function ($L_{\min} \sim 5 \times 10^{33}$ erg s^{-1} Hz^{-1}). We can see that, up to $z = \sim 1$, the quasars will be observable over the entire luminosity range.

Figure 5b shows the peak frequency in the source frame. The decrease of the variance of the peak-frequency distribution beginning at $z = \sim 1.4$ is readily visible. The mean peak frequency for quasars with $z < 1.4$, $\bar{\nu}_{\max}$ ($z < 1.4$), is 11.2 GHz, with $\sigma = 7.0$ GHz. For quasars with $z > 1.4$, we have $\bar{\nu}_{\max}$ ($z > 1.4$) = 6.1 GHz, with $\sigma = 2.0$ GHz; i.e., the standard deviation for this group

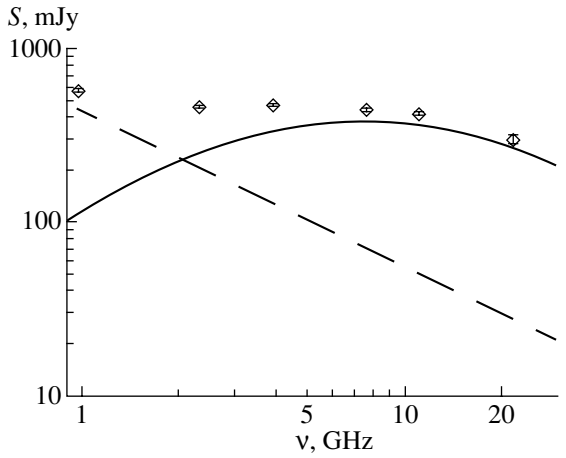

Fig. 2. Separation of the spectrum of 0805 + 046 into components. The diamonds show the initial spectrum, the dashed curve the spectrum of the extended component, and the solid curve the spectrum of the compact component.

of quasars is a factor of 3.5 smaller. The source-rest-frame peak frequencies for these groups of quasars nearly coincide: $\bar{\nu}_{max}(z < 1.4) = 21.0$ GHz, $\sigma = 14$ GHz and $\nu_{max}(z > 1.4) = 20.2$ GHz, $\sigma = 7.1$ GHz. The rest-frame peak frequencies for the BL Lac objects are somewhat lower than for the quasars: $\bar{\nu}_{max}(\mathrm{L}) = 17$ GHz, $\sigma = 1$ GHz. All the data about the peak frequencies are listed in Table 4, which also gives the mean redshifts for each source group.

The variance decrease for distant quasars is due to the absence of sources with low peak frequencies. This could be due to the absence of low-luminosity quasars in this group. If low-luminosity quasars have, on average, lower peak frequencies, the peak frequencies will be bounded from below by a curve that is proportional to the spectral distance, i.e., by a dependence of the form $l_{bol}^2/(1+z)$, which is shown by the dashed curve in Fig. 5b. This also supports the possible weak correlation between the peak frequency ν_{max} and redshift (the correlation coefficient is 0.356, with a significance level smaller than 10%). The peak frequency can depend on the luminosity if the distribution of linear dimensions of the compact components is independent of (or only weakly depends on) the luminosity.

Based on an analysis of the VLBI survey [16, 17], carried out at 2.32 and 8.55 GHz, Popov and Kovalev [15] determined the average size of the central component (core) of a compact radio source to be 2.6 pc. The resulting angular sizes [15, Fig. 3] yield a range of lin-

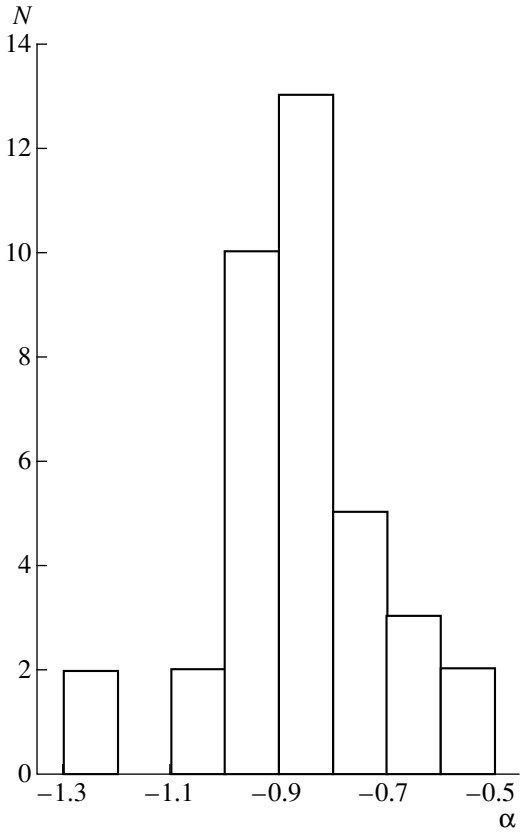

Fig. 3. Distribution of spectral indices α for the extended components.

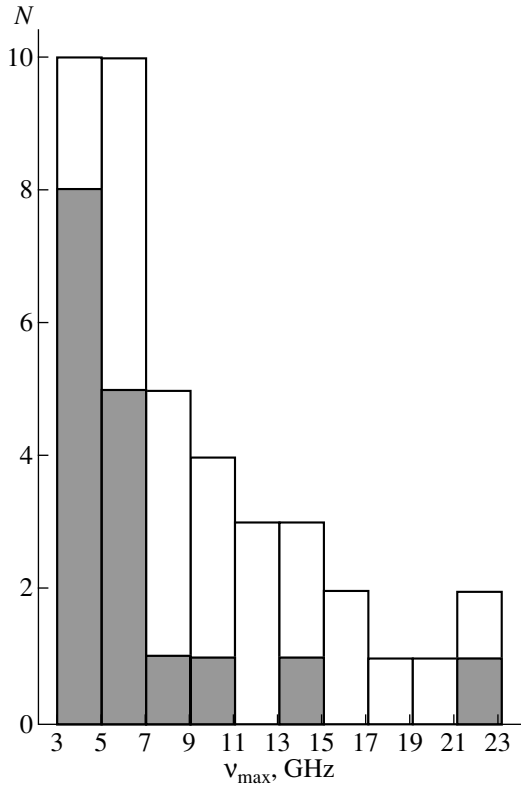

Fig. 4. Distribution of peak frequencies ν_{max} for the spectra of compact components. The sources that had type-5 spectra prior to the component separation (spectra with a flux maximum at 3–23-GHz) are shaded.

Table 3. Spectral parameters of sources with separated components

Name	R.A. (1950.0)	Dec. (1950.0)	Identification	z	S_{max}, mJy	ν_{max}, GHz	A
1	2	3	4	5	6	7	8
0002 + 051	00 02 46.42	05 07 28.00	Q	1.899	226	4.669	–0.801
0019 + 058	00 19 58.12	05 51 24.50	L		286	11.985	–1.280
0026 + 048	00 26 29.11	04 53 00.10	Q	1.633	327	5.611	–1.260
0027 + 056	00 27 11.25	05 38 01.59	Q	1.314	537	22.737	–2.299
0119 + 041	01 19 21.25	04 06 42.02	Q	0.637	1549	12.376	–0.898
0146 + 056	01 46 45.45	05 40 59.59	Q	2.345	1374	7.696	–0.740
0152 + 043	01 52 27.98	04 23 46.71	Q	1.132	256	4.470	–0.735
0231 + 045	02 31 30.47	04 33 39.00	Q	2.06	282	3.085	–1.065
0258 + 058	02 58 55.14	05 50 38.33	Q	2.313	294	4.300	–1.076
0303 + 051	03 03 09.95	05 11 59.35			282	4.657	–0.365
0351 + 045	03 51 46.10	04 32 38.00			239	5.596	–0.587
0355 + 055	03 55 06.68	05 33 55.41			275	6.206	–0.440
0357 + 057	03 57 32.15	05 42 17.70	Q	0.761	467	13.634	–1.192
0409 + 044	04 09 59.90	04 29 56.00			231	5.158	–0.882
0423 + 051	04 23 57.20	05 11 49.00	Q	1.333	574	3.050	–1.479
0430 + 052	04 30 31.51	05 14 59.43	G	0.03	4140	7.942	–0.707
0506 + 056	05 06 45.81	05 37 50.96	L		500	11.203	–0.632
0718 + 042	07 18 45.60	04 12 42.00			578	22.663	–0.753
0801 + 044	08 01 19.40	04 29 36.01			197	4.851	–0.533
0805 + 046	08 05 19.23	04 41 18.30	Q	2.876	383	7.454	–0.729
0830 + 040	08 30 41.56	04 00 49.40			375	17.506	–0.671
1036 + 054	10 36 10.95	05 28 06.52			716	15.904	–1.040
1117 + 044	11 17 08.00	04 26 45.00			211	6.895	–1.046
1204 + 057	12 04 24.42	05 46 33.39			281	13.684	–1.391
1219 + 054	12 19 19.29	05 26 54.39			135	8.369	–0.498
1358 + 046	13 58 17.33	04 39 59.58			126	6.696	–0.876
1402 + 044	14 02 29.91	04 29 54.38	Q	3.202	1071	6.278	–2.274
1509 + 054	15 09 12.17	05 29 28.98	G		916	13.198	–0.390
1541 + 050	15 41 05.00	05 01 44.40	G	0.0398	251	9.926	–1.318
1548 + 056	15 48 06.90	05 36 10.89	Q	1.422	3475	9.793	–0.453
1614 + 051	16 14 08.52	05 06 55.04	Q	3.209	889	5.903	–0.485
1646 + 042	16 46 57.92	04 17 09.58			228	7.922	–0.501
1656 + 053	16 56 05.63	05 19 46.70	Q	0.887	1062	6.396	–1.247
1725 + 044	17 25 56.37	04 29 27.70	Q	0.293	1330	19.079	–0.712
1758 + 046	17 58 36.30	04 38 46.00			249	4.090	–1.156
1926 + 050	19 26 51.69	05 01 41.85			239	9.092	–0.931
2019 + 050	20 19 06.56	05 05 37.66			461	4.227	–0.656
2149 + 056	21 49 07.94	05 38 07.33	Q	0.740	901	4.070	–0.822
2243 + 047	22 43 21.51	04 45 07.68	Q	1.091	366	15.072	–0.869
2259 + 058	2 59 21.58	05 53 05.06			340	6.160	–1.060
2346 + 052	23 46 47.73	05 17 58.93	L		345	10.739	–0.682

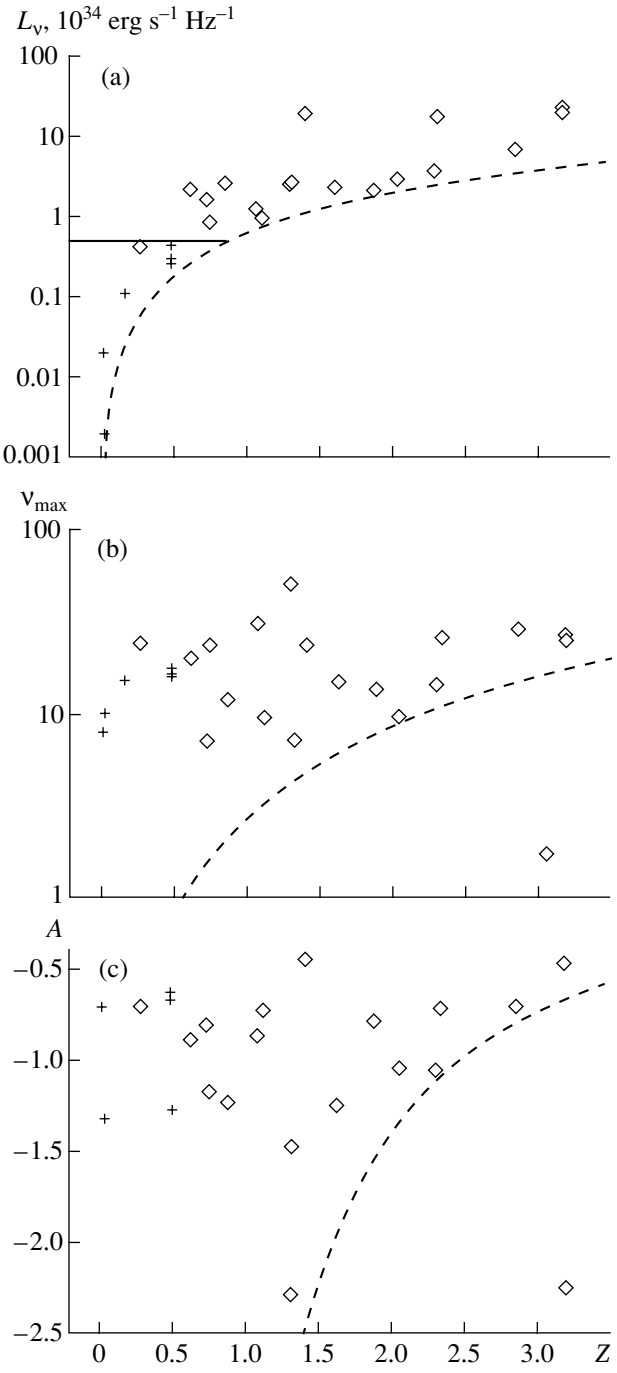

Fig. 5. Spectral characteristics of compact components (diamonds: quasars; crosses: BL Lac objects and galaxies) as functions of redshift z: (a) absolute spectral radio luminosity at the peak frequency L_{max} (dashed line: minimum luminosity that can be detected for sources in the given flux-limited sample; horizontal segment: cutoff of the quasar luminosity function at $L_{min} \sim 5 \times 10^{33}$ erg s^{-1} Hz^{-1}); (b) peak frequency in the source rest frame (dashed curve: dependence of the form $l_{bol}^2/(1+z)$, limiting ν_{max} from below); (c) spectrum curvature in the optically thin region (the parameter A) (dashed curve: dependence of the form $l_{bol}^2/(1+z)$, limiting A from below).

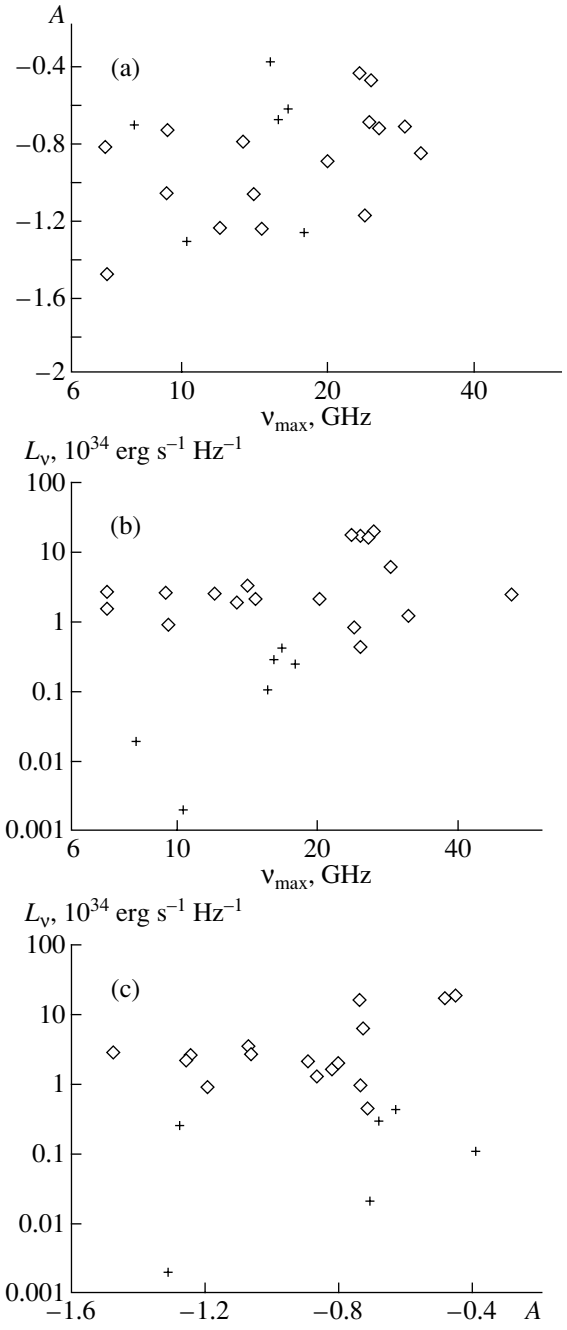

Fig. 6. Spectral characteristics of compact components (diamonds: quasars; crosses: BL Lac objects and galaxies): (a) spectrum curvature in the optically thin region (A) as a function of the peak frequency ν_{max}; (b) absolute radio luminosity at the peak frequency L_{max} as a function of peak frequency ν_{max}; (c) absolute radio luminosity L_{max} as a function of spectrum curvature A.

ear dimensions from 0.8 pc (boundary of the core) to 6.7 pc (components are well separated). Thus, there exist natural upper and lower boundaries for the size distribution for compact components, which likely depend on the type of radio source (QSO, RG, BL) but not on the luminosity of the object.

Table 4. Data on peak frequencies

Radio sources	N	$\bar{z}$	σ	Observer's frame		Source frame	
				$\bar{\nu}_{max}$, GHz	σ	$\bar{\nu}_{max}$, GHz	σ
All QSOs	18	1.62	0.89	8.65	5.7	20.0	11.0
QSO ($z > 1.4$)	9	2.33	0.65	6.1	2.0	20.2	7.1
QSO ($z < 1.4$)	9	0.91	0.34	11.2	7.0	21.0	14.0
L	3	(0.5)	–	11.3	0.6	17.0	1.0

Table 5. Parameters of the sources whose spectra could not be separated into components

Name	R.A. (1950.0)	Dec. (1950.0)	Identification	z	A_0	A_1	A_2
1	2	3	4	5	6	7	8
0237 + 040	02 37 14.51	04 03 29.84	Q	0.978	2.979	−0.158	−0.044
0320 + 045	03 20 37.00	04 35 45.00			2.368	−0.567	0.213
0348 + 049	03 48 15.32	04 57 19.67			2.868	−0.449	
0425 + 048	04 25 08.53	04 50 30.54			2.942	−0.577	0.336
0502 + 049	05 02 43.86	04 55 38.51	Q	0.954	3.012	−0.081	−0.066
0731 + 050	07 31 18.40	05 02 55.86			2.433	−0.071	0.122
0806 + 059	08 06 04.03	05 59 24.05			2.775	−0.721	0.243
0829 + 046	08 29 10.89	04 39 47.63	L	0.18			
0858 + 050	08 58 34.06	05 00 47.10			2.088	0.627	−0.192
1013 + 054	10 13 26.63	05 28 00.50			2.576	−0.930	0.559
1015 + 057	10 15 51.24	05 45 32.90					
1142 + 052	11 42 47.12	05 12 06.03	Q	1.342	2.897	−0.658	0.308
1219 + 044	12 19 49.15	04 29 54.03	Q	0.965	2.799	−0.393	0.585
1228 + 045	12 28 54.40	04 34 36.00			2.490	−0.020	
1237 + 049	12 36 59.94	04 59 33.30			2.624	0.030	
1421 + 048	14 21 38.52	04 48 29.06			2.360	−0.286	0.171
1456 + 044	14 56 29.57	04 28 13.65			3.070	−0.529	0.453
1542 + 042	15 42 29.73	04 17 07.55	Q	2.182	2.973	−0.803	0.398
1557 + 0.43	15 57 33.00	04 21 21.21			2.447	−0.643	0.401
1614 + 042	16 14 44.02	04 16 00.88			2.562	−0.410	−0.055
1642 + 054	16 42 28.53	05 24 06.05			2.878	−0.784	0.237
1936 + 046	19 36 01.87	04 41 19.48			2.742	−0.315	0.194
2114 + 048	21 14 50.80	04 50 27.71					
2121 + 053	21 21 14.82	05 22 27.10	Q	1.941			
2144 + 042	21 44 24.22	04 13 30.60			1.707	0.769	−0.173
2201 + 044	22 01 45.75	04 25 32.46	G	0.028	2.943	−0.643	0.275
2318 + 049	23 18 11.93	04 57 23.63	Q	0.623	2.802	0.144	0.070
2355 + 042	23 55 56.00	04 13 30.00			2.423	−0.423	0.299

Note: Notation in column 4: (Q) QSO, (L) BL Lac object.

Figure 5c demonstrates the lack of a correlation between the spectral curvature in the optically thin region (A) and the redshift. A dependence of the form $l_{bol}^2/(1+z)$ is also shown in Fig. 5c by the dashed curve. The lack of such a correlation is equivalent to the lack of a correlation between the luminosity and spectral index in the optically thin region of the spectrum.

Landau *et al.* [14] reported a significant correlation between the spectral parameters A, B, and C [see (2)] based on simultaneous observations over a wide frequency range (from radio to optical) for a sample of 15 sources. A correlation between the peak flux density S_{max}, peak frequency ν_{max}, and spectral index α in the optically thin region of the spectrum was found in [18].

The parameters C and B correspond to S_{max} and ν_{max}, while the parameter A characterizes the steepness of the spectrum, and can be related to the spectral index.

We have also done a correlation analysis between L_{max} (the absolute luminosity at the maximum of the spectrum), ν_{max}, and A. The input data are presented in Fig. 6. We find a possible correlation between the luminosity and peak frequency (correlation coefficient 0.365), with a confidence level of 10%. The same correlation coefficient for the flux density S_{max} and peak frequency ν_{max} was obtained in [18], though [18] deals with more powerful sources, which have a wider spread of peak frequencies.

We found no correlation between L_{max} and A or between A and ν_{max}, though in [14, 18] such correlations were found with significance levels smaller than 0.01%. What is the origin of this large difference in the properties of these spectral parameters? The strong correlation between S_{max} and α found in [18] is to a considerable extent the result of selection effects: According to the selection criteria imposed, low-luminosity sources with steep spectra were not included in the sample. In our sample, we have made no selection with respect to spectral index, since the sample was formed in accordance with a limiting flux density at a lower frequency than the peak frequencies for nearly all the sources.

We found no correlation between α and ν_{max}, since this correlation is due to objects with high peak frequencies, which are missing from our sample due to the restricted frequency range for the observations and the lower luminosities of the objects. This correlation vanishes after excluding objects with $\nu_{max} > 50$ GHz from the data of [18].

Thus, it is very probable that the distribution of source linear dimensions does not depend on luminosity.

Spectra of the remaining sources. Table 5 lists 28 sources in which we could not separate the spectra into power-law and compact components (objects with spectra of types 1–3). We approximated the spectra of these sources by a logarithmic parabola

$$\log S = A_0 + A_1 \log\nu + A_2 \log\nu^2.$$

For four sources (0829+046, 1015+057, 2114+048, and 2121+053), we were unable to obtain satisfactory approximations. These sources have the largest variability amplitudes among those listed in Table 5. Table 5 contains the source names, right ascensions, and declinations (columns 1–3); identifications and redshifts (columns 4, 5); and approximation coefficients A_0, A_1, and A_2 (columns 5–8). The sources in Table 5 are, on average, fainter in the optical: Almost half the sources are fainter than 20.5^m. Accordingly, redshifts have been measured for less than one-third of these sources (compared to 50% of the sources in Table 3). The mean redshift $\bar{z}$ is 1.0 (with standard deviation 0.7).

The fraction of active objects among these sources is the highest. During the 1.5 years of our observations, we found variability in 60% of these sources. Among the 41 sources with pronounced compact components and peak frequencies lower than 23 GHz, variability was found in only 12 objects. Among the compact components, variable sources have higher peak frequencies: The mean peak frequency $\bar{\nu}_{max}$ is 14 GHz, with $\sigma = 6$ GHz; this considerably exceeds the mean value for the distribution for all the sources ($\bar{\nu}_{max} = 9$ GHz, $\sigma = 5$ GHz).

The variable sources of Table 5 either have even higher peak frequencies or are in a stage of recurrent activity, when several compact components are present simultaneously.

4. CONCLUSIONS

(1) The spectra of the flat-spectrum sources of the complete sample at 0.97–21.7 GHz can be divided into 5 classes. This separation is related to two factors.

The first factor is the peak flux of the extended component at low frequencies compared to the peak flux of the compact component. In sources with spectra of types 2–4 (Fig. 1), the extended component makes the largest contribution to the total emission at frequencies below 4–5 GHz, whereas in sources with spectra of types 1 and 5 (Fig. 1), the emission of the compact component dominates at these frequencies. For 60% of the sources, we could separate the extended and compact components. The spectral-index distribution for the extended components (mean spectral index $\bar{\alpha} = -0.87$, $\sigma_{\bar{\alpha}} = 0.15$) coincides with that for sources with power-law spectra.

The second factor is the activity of a radio source at the epoch of observation. Sources that are at an initial stage of activity—i.e., at an initial phase of evolution of the ejection—have a higher peak frequency and a larger mean relative variability amplitude. These are sources with spectra of types 1 and 2, for which the peak frequency is outside the observed frequency band. Sources with spectra of types 3 and 4 are at a later stage of evolution, their peak frequencies are at centimeter wavelengths, and their variability amplitudes are lower. The mean redshifts of sources with type 1–4 spectra are approximately the same ($\bar{z} = 1.2$–1.3), enabling us to compare frequencies in the observer's frame. This behavior of the variable sources is consistent with all standard variability models.

(2) As a rule, sources with large redshifts ($\bar{z} = 2.03$) have no appreciable extended component, a very small scatter of peak frequencies, and little or no variability on timescales of 1.5 years.

(3) We have confirmed the weak correlation between the luminosity at the peak frequency L_{max} and the peak frequency ν_{max} in the spectra of compact components found in [14, 18]. We suggest that this correla-

tion is a consequence of the lack of dependence of the distribution of source linear dimensions on their luminosity.

(4) We have found no correlation between L_{max} and the curvature parameter A or between A and ν_{max}. We have demonstrated that the correlations between these parameters found in [18] are a consequence of selection effects.

ACKNOWLEDGMENTS

This work was supported by the Russian Foundation for Basic Research (project no. 98-02-16428), a grant of the "Universities of Russia" (no. 5561), and a grant of the Federal Program in Science and Technology "Astronomy" (no. 1.2.5.1).

REFERENCES

1. G. B. Sholomitskiĭ, IAU Bull. Variable Stars **83**, 1 (1965).
2. W. A. Dent, Science **148**, 1458 (1965).
3. M. Bondi, L. Padrielli, R. Fanti, *et al.*, Astron. Astrophys., Suppl. Ser. **120**, 89 (1996).
4. B. H. Andrew, J. M. MacLeod, G. A. Harvey, and W. J. Medd, Astron. J. **83**, 863 (1978).
5. H. D. Aller, M. E. Aller, G. E. Latimer, and P. E. Hodge, Astrophys. J., Suppl. Ser. **59**, 513 (1985).
6. H. Terasranta, M. Tornikoski, E. Valtaoja, *et al.*, Astron. Astrophys., Suppl. Ser. **94**, 121 (1992).
7. G. R. Romero, G. Surpi, and H. Vicetich, Astron. Astrophys. **301**, 64 (1995).
8. V. R. Amirkhanyan, A. G. Gorshkov, A. A. Kapustkin, *et al.*, *Catalog of Sources from Zelenchuk Sky Survey in the Declination Range 0°–14°* [in Russian] (Mosk. Gos. Univ., Moscow, 1989).
9. A. M. Botashev, A. G. Gorshkov, V. K. Konnikova, and M. J. Mingaliev, Preprint No. 132, SAO RAN (Spec. Astrophys. Obs., Russian Academy of Sciences) (1998).
10. A. G. Gorshkov and V. K. Konnikova, Astron. Zh. **72**, 291 (1995).
11. R. A. Nizhel'skiĭ, Otchet Spets. Astrofiz. Obs. (1996), p. 57.
12. A. B. Berlin, A. A. Maksyasheva, N. A. Nizhel'skiĭ, *et al.*, in *Proc. XXVII Radio Astronomy Conference*, St. Petersburg (1997), Vol. 3, p. 115.
13. G. A. Seielstad, T. J. Pearson, and A. C. S. Readhead, Publ. Astron. Soc. Pac. **95**, 842 (1983).
14. R. Landau, B. Golisch, T. J. Jones, *et al.*, Astrophys. J. **308**, 78 (1986).
15. M. V. Popov and Yu. Yu. Kovalev, Astron. Zh., 2000 (in press).
16. A. L. Fey, A. W. Clegg, and E. B. Fomalont, Astrophys. J., Suppl. Ser. **105**, 299 (1996).
17. A. L. Fey and P. Charlot, Astrophys. J., Suppl. Ser. **111**, 95 (1997).
18. E. Valtaoja, S. Haarala, H. Lehto, *et al.*, Astron. Astrophys. **203**, 1 (1988).

Translated by G. Rudnitskiĭ